ChemPubSoc Europe

DOI: 10.1002/open.201900275

Open Access ChemistryOPEN Full Papers

Facile and Direct Preparation of Ultrastable Mesoporous Silica with Silver Nanoclusters: High Surface Area

Tariq Aqeel*[a] and Ali Bumajdad[b]

We report the successful direct synthesis of an ultrastable mesoporous silicon dioxide framework containing silver nanoclusters using a modified true liquid crystal templating method. Our modification produced an extraordinary material with a high average Brunauer-Emmett-Teller specific surface area of 1785 $m^2 g^{-1}$ – the highest reported surface area to date – and an ultrastable mesoporous structure, which has been stable for nine years so far. This method eliminates the need for reduction of silver oxide into metallic silver and restricts the growth of silver clusters. The silver nanoclusters, with an average size of 1 nm, occupy the pores and walls of the framework. Analysis of the material using nitrogen adsorption/desorption method, high-resolution transmission electron microscopy, X-ray diffractometry, energy-dispersive X-ray diffractometry, X-ray photoelectron spectroscopy, and scanning electron microscopy is discussed herein.

1. Introduction

Please include High Surface Area in the title? Mesoporous SiO_2 (m-SiO_2) structures are well known for their broad range of applications in catalysis, sorption, molecular sieving, filtration, redox reactions, and nanocasting; furthermore, they facilitate the formation of nanotubes, nanowires, and nanoclusters.[1] Recently, m-SiO_2 structures have been employed in the production of clean energy.[2] The syntheses of nanoclusters, nanoparticles, nanotubes, and nanowires in mesoporous structures involve several steps and require a well-ordered, relatively stable mesoporous material with thick walls that can withstand solvolysis and multiple heat treatments.[3] The stability of the mesoporous material to solvolysis is especially important for the introduction of clusters using wet impregnation methods. The thermal stability of the mesoporous material is also important for the removal of organic supporting scaffolds (templates),[4] and the transfer and sintering of the nanoclusters/particles into their metallic or oxide forms.[5]

In this work, we modified the original true liquid crystal templating (TLCT) method by eliminating solvolysis of the noble metal precursor,[6] as well as the subsequent reduction and calcination steps. Instead, we merely introduced the framework (SiO_2) and metal (Ag) precursors directly in a one-pot synthesis protocol. In addition, we extended the ageing step to 3 d at 30 °C; this induced further condensation of the framework, which increased the overall stability of the structure, as previously reported,[7] while the original method required 2 d at 25 °C.[6] The modified method yielded an extraordinary mesoporous silica that contained 1-nm silver nanoparticles (m-Ag–SiO_2) with a high average specific surface area of 1780 $m^2 g^{-1}$ and an ultrastable mesoporous structure. Remarkably, the porous structure of the m-Ag–SiO_2 material has been stable for approximately nine years. This method is advantageous for controlling the sizes of the Ag nanoparticles, first by confinement and then by diffusion into the silica walls; this also limits metallic leaching during liquid catalysis or sorption testing, as studied by Wang.[8] The rate of Ag-particle diffusion into the silicate matrix reportedly increases with increasing temperature,[2] and Ag migration depends on the reducing/oxidising atmosphere, substrate type, and temperature.[9] Restricting the Ag-cluster size to lie within the range of quantum dimensions,[9,10,11] and altering the shape and type of support material can lead to a variety of fascinating properties.[12,13] Previous attempts to synthesise m-Ag–SiO_2 in a one-pot procedure used a liquid crystal templating (LCT) method, in which the precursor and the surfactant together dictated the product morphology (pore order arrangement). On the other hand, the porous structure is determined only by the surfactant arrangement, and forms a mesophase (liquid crystal phase) in the TLCT method.[1] These previous LCT syntheses produced materials that exhibited larger Ag-particle sizes with undefined locations on/within the matrix and lower specific surface areas (1000 $m^2 g^{-1}$[14] and 450 $m^2 g^{-1}$[15]), while the m-SiO_2 framework lacked long-range order.[15] Other research groups have attempted to introduce Ag precursors by impregnating pre-synthesised m-SiO_2 structures.[16–33] The average Ag nanoparticle sizes in these materials varied from 2 to 50 nm, and the Brunauer-Emmett-Teller (BET) specific surface areas ranged from 300–800 $m^2 g^{-1}$. Curiously, no information was provided regarding the shelf life stabilities of these structures. Overall, m-Ag–SiO_2 – with nanosized silver particles encompassed in a silica matrix – presents unique properties and effects, including

[a] Dr. T. Aqeel
Department of Science, College of Basic Education
The Public Authority of Applied Education and Training (PAAET) P.O. Box 23167, Safat 13092, Kuwait
Phone: (965) 2221266 Extension: 6269
E-mail: tm.aqeel@paaet.edu.kw

[b] Prof. A. Bumajdad
Department of Chemistry, Faculty of Science, Kuwait University P.O. Box 5969, Safat 13060, Kuwait
Phone: (965) 24987453

anti-bacterial properties,[23–24] aggressive behaviour towards cancer cells,[25] enhanced analyte sensing ability,[26] pesticide detection,[27] catalysis,[28–29] photocatalysis,[30] micro-jet applications,[31] selective removal of sulphur compounds (adsorption),[32] and water treatment.[33] The facile TLCT method we have developed to produce m-Ag–SiO_2 will benefit such properties and applications.

2. Results and Discussion

2.1. Nitrogen Sorption Study

Samples of m-Ag–SiO_2 acquired immediately after calcination, and of the same calcined product after 9 y of storage, were subjected to N_2-sorption tests. The results are shown in Figure 1. According to the IUPAC classification system, both isotherms lay between those of type I-b (wide micropores) and IV-b (narrow mesopores), and did not show hysteresis during the desorption cycle, indicating that the pore sizes are below the critical size. Hence, the material has uniformly sized pores below 4 nm.[34] The samples exhibited narrow pore size distributions in the 2–3 nm range, (Figure 1, insets (c) and (d)) and an average pore diameter of 2.4 nm. Hence, m-Ag–SiO_2 was deemed mesoporous according to IUPAC classification.[34] Moreover, the pore distribution was unchanged after 9 y, as evidenced by Figure 1, insets (c) and (d), indicating that m-Ag–SiO_2 has an ultrastable structure. The BET specific surface areas of the material determined in 2008 and after 9 y of storage were 1835 and 1735 $m^2 g^{-1}$, respectively, with an average value of 1785 $m^2 g^{-1}$, which is very high compared to that of mesoporous materials obtained by the original TLCT method,[6] and superior to that of other mesoporous SiO_2–Ag products reported in the literature.[16–33] The difference between the two BET values was approximately 5.5%, which can be attributed to nine years of storage that may have resulted in slight structural degradation, or a measurement error (human or instrumental). The average Barrett-Joyner-Halenda (BJH) specific pore volume of m-Ag–SiO_2 was also higher (0.8 $cm^3 g^{-1}$) than those reported in the literature for other (0.1–0.7 $cm^3 g^{-1}$) SiO_2–Ag products.[13,16–33] The adsorbed volumes determined from the two isotherms lay between 250 and 500 $cm^3 g^{-1}$, which clearly demonstrated the higher specific surface area of the m-Ag–SiO_2 sample compared to that of typical m-SiO_2 prepared by the original TLCT method;[6] the specific pore volume of a typical m-SiO_2 sample is usually in the 200–350 $cm^3 g^{-1}$ range.

2.2. X-Ray Diffraction Studies

Figure 2 displays the narrow-angle X-ray diffraction (XRD) patterns of the calcined m-Ag–SiO_2. The main Bragg diffraction peaks assigned to hexagonal pore packing are indicated by arrows. The presence of the main diffraction peak corresponds to the (100) plane and the second peak corresponds to the (110) plane arising from pores with long-range order (also confirmed by transmission electron microscopy (TEM), *vide infra*). The XRD patterns also revealed *d*-spacings of 31.5 Å, distances, a_0, between successive pore centres of 36.5 Å, and wall thicknesses of 12.5 Å (calculated from the pore diameter of 2.4 Å obtained from the N_2-sorption study (Figure 1)). Moreover, the XRD patterns showed that the hexagonal pore packing was intact even after 9 y of storage (Figure 2 (b)).

The wide-angle XRD pattern displayed in Figure 3 indicates that Ag nanoclusters had formed. Figure 3(a) displays a broad peak in the 20–35° 2θ range, which corresponds to the amorphous m-SiO_2 matrix, while the low-intensity peaks in the 30–80° 2θ range correspond to metallic Ag clusters. The four diffraction planes of the crystalline Ag particles are indicated by arrows and are consistent with those reported previously.[14,15,20,35] These low-intensity silver nanoparticle peaks are indicative of very small particle sizes, as also confirmed by TEM (Figure 4(c) and (d)), while the metallic nature of Ag was confirmed by X-ray photoelectron spectroscopy (XPS) (*vide infra*). Hence, we were

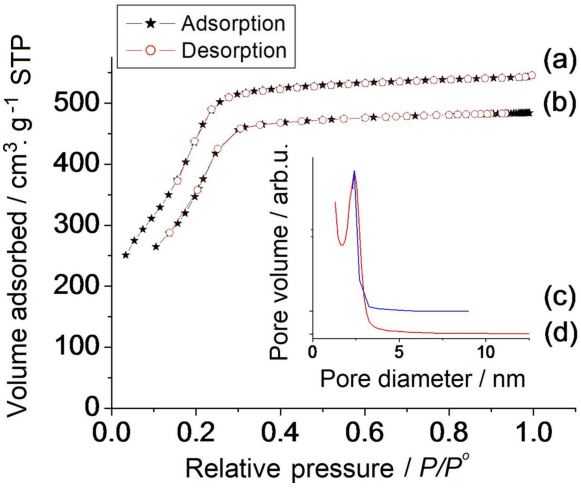

Figure 1. (a) Initial isotherm of the calcined m-Ag–SiO_2 acquired in 2008. (b) Isotherm of the same sample acquired after 9 y of storage. The inset shows the BJH pore diameter distributions obtained in (c) 2008 and (d) 2017.

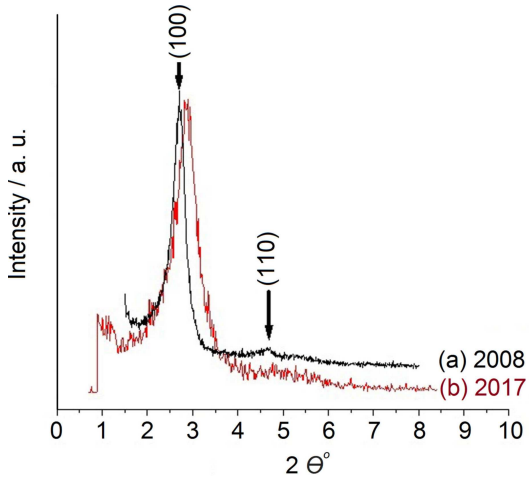

Figure 2. Narrow-angle XRD patterns of hexagonal m-Ag–SiO_2 acquired in (a) 2008 immediately after calcination for 8 h at 500 °C and (b) 2017, after storage for 9 y.

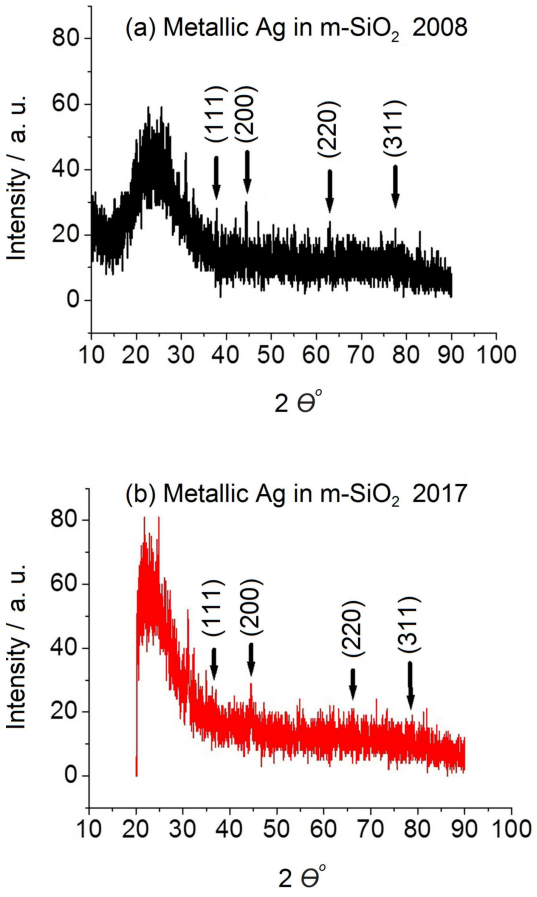

Figure 3. Wide-angle XRD patterns showing the diffraction planes (indicated by arrows) of metallic Ag in the mesoporous SiO_2 matrix acquired in (a) 2008 immediately after calcination at 500 °C for 8 h and (b) 2017, following 9 y of storage.

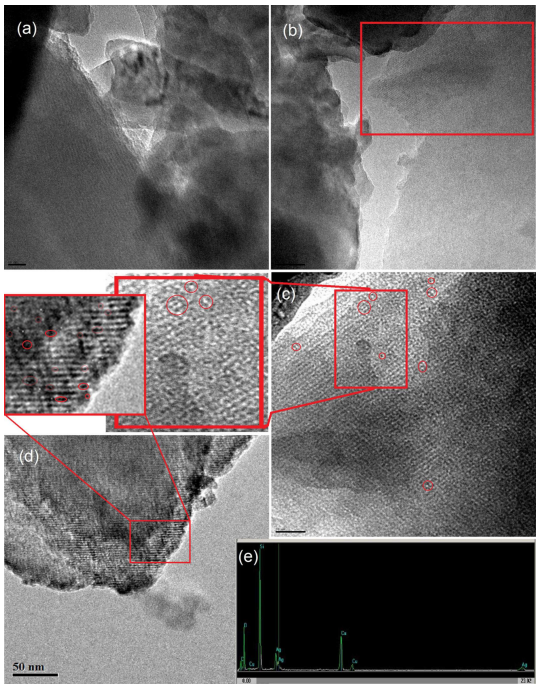

Figure 4. TEM images of m-Ag–SiO_2. (a) and b) display different sections of the sample, and (c) shows an enlarged view of the region enclosed by the red rectangle in image (b). A small section of image (c) is enlarged to show Ag-particle diffusion into the walls adjacent to the pore openings. The scale bars are 20 nm in (a), (b), and (c). (d) HRTEM image of m-Ag–SiO_2 acquired in 2017 and (e) the corresponding EDX spectrum.

unable to apply the Scherrer equation to calculate the Ag-particle size. Figure 3(b) shows the XRD pattern of the m-Ag–SiO_2 sample acquired after 9 y. The similarities between the XRD patterns of m-Ag–SiO_2 acquired in 2008 and 2017 indicate that this material is ultrastable.

2.3. High-Resolution TEM and Energy-Dispersive X-Ray Diffractometry

High-resolution TEM (HRTEM) images acquired after calcination clearly revealed the long-range pore order in the sample, as shown in Figs. 4(a)–(d); the parallel lines indicate the cylindrical tube structure of the pores. In addition, the average wall thickness and pore size were very close to those determined by narrow-angle XRD and N_2-sorption testing. The black spots within the red frame in Figure 4(b), in the few selected red circles in Figure 4(c), and Figure 4(d) correspond to Ag clusters. The silver nanoclusters are 0.8–1.2 nm in size and appear to occupy the pores as well as having diffused into the walls adjacent to the pore openings, which is evident in the magnified image shown in Figure 4(c and d). We believe that the Ag precursor became trapped between the templating material and the SiO_2 precursor during synthesis prior to calcination (at temperatures up to 100 °C);[36] Ag_2O was subsequently formed as an intermediate product at temperatures above 350 °C during conversion into the metallic Ag particles,[14,36] where they diffused into the scaffold walls.[8,10,11] This diffusion suppressed the aggregation and growth of Ag particles into larger clusters. Therefore, this method eliminates the need for a reduction step to convert silver oxide into its metallic form; additionally, it confines the size of the silver nanoclusters.[31,32]

Figures 4(d) and (e) show an HRTEM image and the corresponding energy-dispersive X-ray (EDX) spectrum of m-Ag–SiO_2, respectively, acquired after 9 y of storage. The material clearly maintained the long-range order of the Ag-nanoparticle-containing pores, even after long-term storage (Ag clusters that were well embedded in the framework are clearly visible in the enlarged image (Figure 4(d)). The corresponding EDX spectrum (Figure 4(e)) revealed the presence of silicon, oxygen, and silver on the surface and subsurface of the sample, as well as Cu K and L lines that correspond to the sampling grid.

2.4. Scanning Electron Microscopy and EDX (Quantification)

Figure 5 displays a scanning electron microscopy (SEM) image of the calcined m-Ag–SiO_2 acquired after storage for 9 y, which shows the selected area that was targeted by the EDX beam (indicated by the square), the corresponding spectra, and

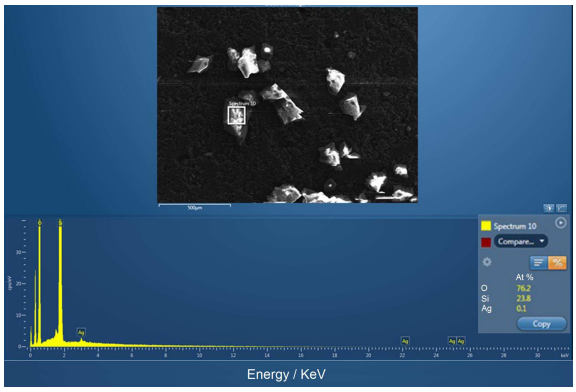

Figure 5. SEM image/EDX spectrum of m-Ag–SiO_2 and a table (inset, bottom right) listing the at% values of the elements presents in the sample after 9 y of storage.

elemental quantification (bottom right inset in Figure 5). After converting the atomic percentages (at%) to weight percentages (wt%), the m-Ag–SiO_2 sample was found to contain 0.57 wt% Ag. When compared to the composition of the as-prepared sample (0.64%), the material exhibited excellent compositional stability during storage.

2.5. X-Ray Photoelectron Spectroscopy

The oxidation states of Si and Ag in the m-Ag–SiO_2 sample and the bonding types present were investigated by XPS after 9 y of storage. The symmetrical Si XPS spectrum shown in Figure 6(a), which displays Si-related peaks at 103.4 and 104.3 eV that correspond to Si^{4+} $2p_{3/2}$ and $2p_{1/2}$ orbital splitting, respectively, indicate the presence of Si–O bonds in the SiO_2 framework.[8,9,38] On the other hand, the O1s XPS peak shown in Figure 6(b), centred at 533.3 eV, corresponds to O^{2-} atoms in SiO_2.[37,38,39] In addition, Ag peaks (Figure 6(c)), at 368.4 and 374.4 eV, correspond to Ag $3d_{5/2}$ and $3d_{3/2}$ orbital splitting, respectively,[40] confirming the existence of metallic Ag nanoclusters within the mesoporous SiO_2 matrix. However, Ag–O bonds (at binding energies 377 or 371 eV) were not observed.[40] Moreover, XPS quantification revealed that 0.64 wt% Ag was present in the m-Ag–SiO_2 sample. These results, together with the EDX quantification data confirmed that the Ag-particle concentration did not change over 9 y, which is possibly due to the entrapment of the Ag particles inside the silica walls.

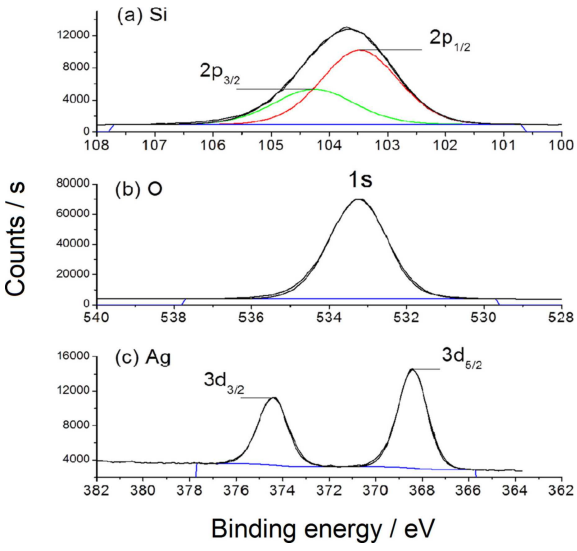

Figure 6. (a) Si, (b) O, and (c) Ag XPS spectra of m-Ag–SiO_2 after 9 y of storage.

3. Conclusions

The robustness of a mesoporous SiO_2 structure is crucial for its use in catalysis and during the synthesis of nanotubes, nanowires, or nanoclusters. Herein, we report for the first time the direct preparation of a mesoporous SiO_2 framework containing silver nanoparticles using a modified TLCT method. Our method introduced silica/metal precursors during synthesis, and the as-synthesised material was aged at 30 °C for 3 d (instead of 25 °C for 2 d according to the original TLCT method). This method yielded a hexagonal mesoporous material with a higher specific surface area than the original TLCT-prepared mesoporous product. This product also exhibited an ultrastable mesoporous structure that remained unchanged for 9 y. The material had an average BET specific surface area of 1785 $m^2 g^{-1}$, mean pore size of 2.4 nm, and an average BJH specific pore volume of 0.84 $cm^3 g^{-1}$. The 0.6 wt% loading of 1-nm-diameter silver nanoclusters occupied the pores (by confinement) and walls of the SiO_2 framework (by entrapment). To the best of our knowledge, this method produced the highest surface area reported so far for m-Ag–SiO_2.

Experimental Section

Synthesis

A modification of Attard's TLCT method [6] was used to synthesise the m-Ag–SiO_2 material. Initially, silver nitrate (0.008 g (0.047 mmol), 99%; Aldrich; Ag precursor) was stirred in methanol (1 mL; Fisher Scientific) at 25 °C for 5 min. Cetyltrimethylammonium bromide (1.0 g (2.744 mmol), Aldrich; CTAB) was added to methanol (1.5 mL) and aqueous hydrochloric acid (1.4 mL, pH 2) in a round bottom flask. A viscous solution was obtained at the isotropic liquid/hexagonal mesophase boundary on heating this solution at 40 °C on a rotary evaporator at slightly reduced pressure. Tetramethoxysilane (2.046 g (13.441 mmol), 98%; Aldrich; SiO_2 precursor) and the Ag/methanol precursor were then added to the mesophase, after which it was heated at 40 °C at reduced pressure until the hexagonal mesophase was re-established. The as-synthesised sample was aged for 3 d at 30 °C and calcined at 500 °C for 8 h under a flow of air at a rate of 3 °C min^{-1}. These quantities were calculated to introduce 0.64% (w/w) of Ag into m-SiO_2. All reagents were used as received, except for the alcohols, which were stored over 4 Å molecular sieves.

Shelf Life Stability Testing

Approximately 1 g of the calcined sample was placed in a glass vial and covered with a plastic lid to protect against dust. The sample was then placed in a storage cabinet under ambient conditions (atmospheric pressure and humidity) at room temperature (25 °C). After storage for 9 y, the sample was re-examined by TEM, N_2-sorption testing, wide- and narrow-angle XRD, SEM, EDX, and XPS.

Characterisation Methods

XRD experiments were conducted on a *D8* single sampler using Cu Kα radiation (1.5418 Å) at 40 mA and 40 kV. Narrow-angle scanning parameters include: numbers of steps = 659, step size = 0.01°, and dwell time per step = 0.50 s. Wide-angle scanning parameters include: number of steps = 7700, step size = 0.01°, and dwell time per step = 0.20 s. A diversion slit at 0.05° and an anti-scattering slit at 0.50° were used for both types of scans. N_2-sorption experiments were conducted using a Micrometrics 2010 instrument with N_2 gas at −196 °C and He as the back-fill gas. The SiO_2 materials were dehydrated for 3 h under vacuum at 160 °C prior to any N_2-sorption experiment. The BJH method was used to determine pore size distributions from the adsorption branches of the N_2-sorption isotherms. In 2008, HRTEM images were acquired on a JEOL-JEM 2010 instrument operating at 200 kV and fitted with a Gatan Orius SC 1000 detector, and in 2017 on a JEOL-JEM 2011 electron microscope fitted with an Oxford link ISIS SemiSTEM EDX system and a LaB6 filament operating at 250 kV. A Gatan 794 CCD camera was used for image recording. TEM samples were suspended in methanol or ethanol or acetone and transferred to Cu TEM grids using capillary glass tubes. The HRTEM images were analysed using ImageJ software. XPS was performed on a Thermo ESCALAB 250Xi spectrometer with monochromated Al–K_α radiation (1486.6 eV). The Avantage data system was used to record and process spectra. The sample was introduced by a sample holder into the preparation chamber. High vacuum was then achieved by degassing, after which the sample was transferred to the analysis chamber. Spectra were acquired at a pass energy of 20 eV, dwell time of 100 ms, step size of 0.1 eV, and 10^{-9} Torr pressure. All binding energies were referenced against the C 1s peak (284.6 eV) of adventitious carbon. The standard charge-compensation mode was used to neutralise the charge build-up on the surface of the insulating layer with a flood gun.

Acknowledgements

This project was funded by the Public Authority of Applied Education and Training (PAAET), Kuwait (Project No. BE-15-04 entitled "Using Mesoporous Materials to Absorb Sulphur Compounds from Kuwaiti Petroleum Products"). Assistance provided by Kuwait University for the XPS (Project No. GS01/05), XRD (Project No. GS03/01) and N_2-sorption experiments (Project No. GS01/01) is acknowledged. We would like to thank Dr Heather F. Green (University of Cambridge) for acquiring the recent TEM, SEM, and EDX data (Project No. FAO., Dr Tariq Aqeel). We would like also thank Dr Mahmood Ardakani at Imperial College for the original TEM data. We would like to thank Editage (www.editage.com) for English language editing.

Conflict of Interest

The authors declare no conflict of interest.

Keywords: silver nanoclusters · high surface area · long shelf life nanoparticles · ultrastable mesoporous SiO_2

[1] A. A. Taguchi, F. Schüth, *Microporous Mesoporous Mater.* **2005**, *77*, 1–45.
[2] N. Linares, A. M. Silvestre-Albero, E. Serrano, J. Silvestre-Albero, J. J. García-Martínez, *Chem. Soc. Rev.* **2014**, *43*, 7681–7717.
[3] T. Linssen, K. Cassiers, P. Cool, E. F. Vansant, *Adv. Colloid Interface Sci.* **2003**, *103*, 121–147.
[4] F. Kleitz, W. Schmidt, F. Schüth, *Microporous Mesoporous Mater.* **2003**, 65, 1–29.
[5] J. Y. Ying, C. P. Mehnert, M. S. Wong, *Angew. Chem. Int. Ed.* **1999**, *38*, 56–77.
[6] G. S. Attard, J. C. Glyde, C. G. Göltner, *Nature* **1995**, *378*, 366–368.
[7] T. Aqeel, A. Bumajdad, *J. Porous Mater.* **2017**, 25, 1237–1243.
[8] P. W. Wang, *J. Vac. Sci. Technol. A* **1996**, *14*, 465–470.
[9] M. X. Yang, P. W. Jacobs, C. Yoon, L. Muray, E. Anderson, D. Attwood, Somorjai, *Catal. Lett.* **1997**, *45*, 5–13.
[10] S. V. Serezhkina, L. T. Potapenko, Y. V. Bokshits, G. P. Shevchenko, V. V. Sviridov, *Glass Phys. Chem.* **2003**, *29*, 5, 484–489.
[11] M. Dubiel, H. Hofmeister, G. L. Tan, K. D. Schicke, E. Wendler, *Eur. Phys. J. D* **2003**, *24*, 361–364.
[12] K. Zhao, C. Wu, Z. Deng, Y. Guo, B. Peng, *RSC Adv.* **2015**, *5*, 52726–52736.
[13] H. Yu, Y. Zhu, H. Yang, K. Nakanishi, K. Kanamori, X. Guo, *Dalton Trans.* **2014**, 43, 12648–12656.
[14] Z. Qu, X. Zhang, F. Yu, J. Jia, *Microporous Mesoporous Mater.* **2014**, *188*, 1–7.
[15] L. Han, H. Wei, B. Tu, D. Zhao, *Chem. Commun.* **2011**, *47*, 8536–8538.
[16] V. S. Gurin, V. P. Petranovskii, M. A. Hernandez, N. E. Bogdanchikova, A. A. Alexeenko, *Mater. Sci. Eng. A* **2005**, *391*, 71–76.
[17] W. Cai, Z. Lide, *J. Phys. Condens. Matter* **1997**, *9*, 7257–7267.
[18] W. Cai, H. Hofmeister, T. Rainer, W. Chen, *J. Nanopart. Res.* **2001**, *3*, 443–453.
[19] S. Besson, T. Gacoin, C. Ricolleau, J.-P. Boilot, *Chem. Commun.* **2003**, 360–361.
[20] J. Hou, B. Yu, E.-G. Liu, W. Dong, P.-C. Lu, Z. Wang, V. C. Yang, J.-B. Gong, *RSC Adv.* **2016**, *6*, 95263–95272.
[21] J. Yang, F. Zhang, Y. Chen, S. Qian, P. Hu, W. Li, Y. Deng, Y. Fang, L. Han, M. Luqman, D. Zhao, *Chem. Commun.* **2011**, *47*, 11618–11620.
[22] G. Cui, Z. Sun, H. Li, X. Liu, Y. Liu, Y. Tian, S. Yan, *J. Mater. Chem. A* **2016**, *4*, 1771–1783.
[23] Q. Tang, J. Liu, L. Kumar Shrestha, K. Ariga, Q. Ji, *ACS Appl. Mater. Interfaces.* **2016**, *8*, 18922–18929.
[24] Y. Tian, J. Qi, W. Zhang, Q. Cai, X. Jiang , *ACS Appl. Mater. Interfaces* **2014**, *6*, 12038–12045.
[25] Z. Wang, Z. Chang, M. Lu, D. Shao, J. Yue, D. Yang, M. Li, W.-F. Dong, *ACS Appl. Mater. Interfaces* **2017**, *9*, 30306–30317.
[26] Q. Zhu, F. Teng, Z. Wang, Y. Wang, N. Lu, *ACS Appl. Nano Mater.* **2019**, *2*, 3813–3818.
[27] J. Zhao, L. Long, G. Weng, J. Li, J. Zhu, J.-W. Zhao, *J. Mater. Chem. C* **2017**, *5*, 12678–12687.
[28] M. N. Khrizanforov, S. V. Fedorenko, A. R. Mustafina, K. V. Kholin, I. R. Nizameev, S. O. Strekalova, V. V. Grinenko, T. V. Gryaznova, R. R. Zairov, R. Mazzaro, V. Morandi, A. Vomiero, Y. H. Budnikova, *Dalton Trans.* **2018**, *47*, 9608–9616.
[29] J. Han, P. Fang, W. Jiang, L. Li, R. Guo, *Langmuir* **2012**, *28*, 4768–4775.
[30] R. Nain, S. Dobhal, P. Bidaliya, G. Saini, B. Pani, S. Sirohi, *RSC Adv.* **2018**, *8*, 20287–20294.
[31] D. Vilela, A. C. Hortelao, R. Balderas-Xicohténcatl, M. Hirscher, K. Hahn, X. Ma, S. Sánchez, *Nanoscale*, **2017**, *9*, 13990–13997.
[32] K. Fujiwara, Y. Kuwahara, Y. Sumida, H. Yamashita, *J. Mater. Chem. A* **2017**, *5*, 25431–25437.
[33] R. Das, C. D. Vecitis, A. Schulze, B. Cao, A. F. Ismail, X. Lu, J. Chen, S. Ramakrishna, *Chem. Soc. Rev.* **2017**, *46*, 6946–7020 and references within.

[34] M. Thommes, K. Kaneko, A. V. Neimark, J. P. Olivier, F. Rodriguez-Reinoso, J. Rouquerol, K. S. W. Sing, *Pure Appl. Chem.* **2015**, *87*, 1051–1069.
[35] N. Mnasri, C. Charnay, L. C. De Ménorval, Y. Moussaoui, E. Elaloui, J. Zajac, *Microporous Mesoporous Mater.* **2014**, *196*, 305–313.
[36] G. I. N. Waterhouse, G. A. Bowmaker, J. B. Metson, *Phys. Chem. Chem. Phys.* **2001**, *3*, 3838–3845.
[37] M. Kuemmel, D. Grosso, C. Boissière, B. Smarsly, T. Brezesinski, P. A. Albouy, H. Amenitsch, C. Sanchez, *Angew. Chem. Int. Ed.* **2005**, *44*, 4589–4592.
[38] G. Larrieu, E. Dubois, X. Wallart, X. Baie, J. Katcki, *J. Appl. Phys.* **2003**, *94*, 7801–7810.
[39] B. Akhavan, K. Jarvis, P. Majewski, *RSC Adv.* **2015**, *5*, 12910–12921.
[40] M. Gozdziewska, G. Cichowicz, K. Markowska, K. Zawada, E. Megiel, *RSC Adv.* **2015**, *5*, 58403–58415.

Manuscript received: September 10, 2019
Revised manuscript received: November 7, 2019